NANO LETTERS

October 23, 2024
Volume 24, Number 42
pubs.acs.org/NanoLett

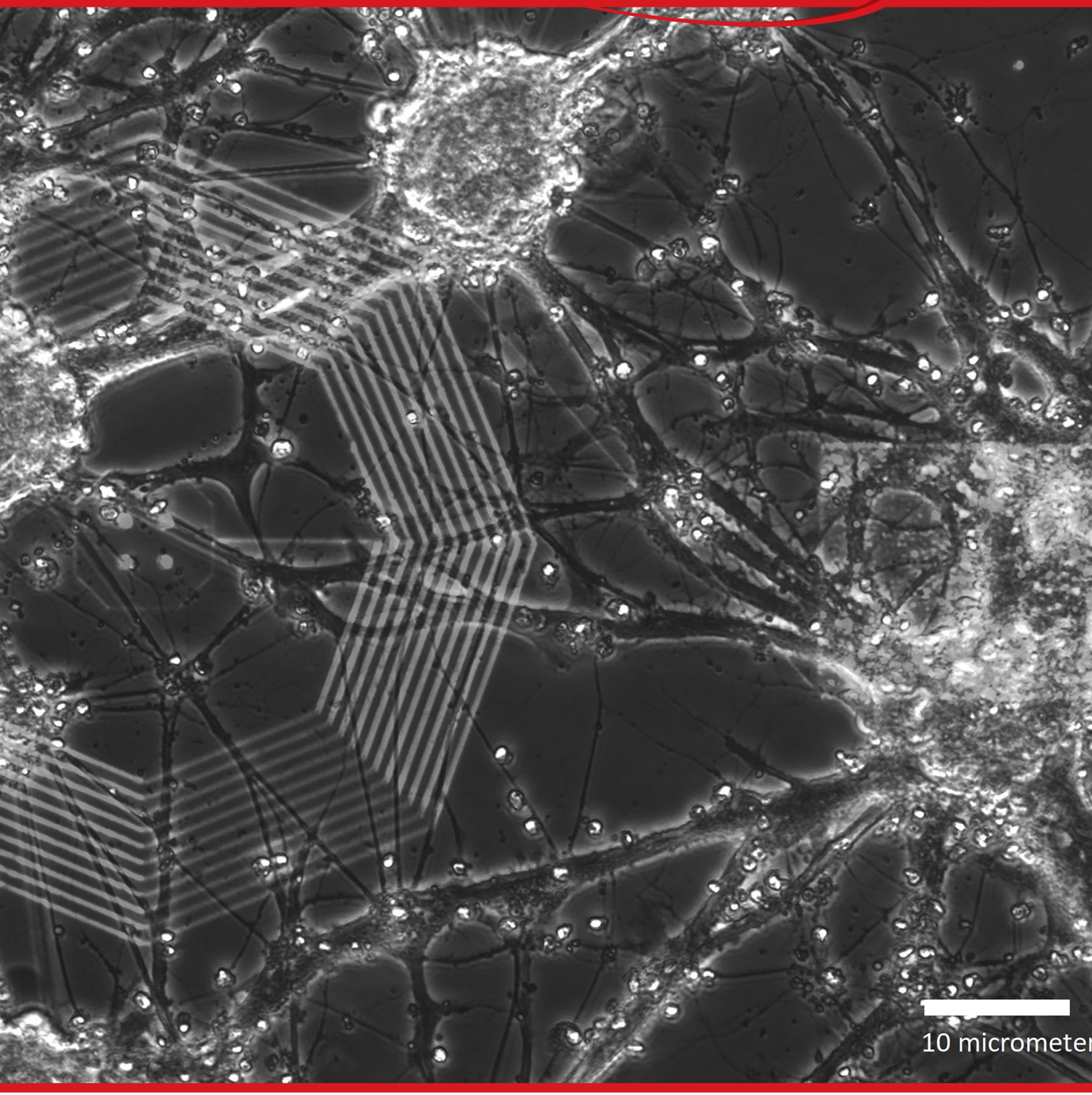


ACS Publications
Most Trusted. Most Cited. Most Read.

www.acs.org

NANO LETTERS



pubs.acs.org/NanoLett
Letter

# Magnetic Detection of Neural Activity by Nanocoil Transducers

Ilhan Bok, Jack Phillips, Tianxiang Zhu, Jennifer Lu, Elizabeth Detienne, Eduardo Andrade Lima, Benjamin P. Weiss, Alan Jasanoff,* and Aviad Hai*

Cite This: *Nano Lett.* 2024, 24, 13147−13152



**ABSTRACT:** Electrophysiological recordings from brain cells are performed routinely using implanted electrodes, but they traditionally require a wired connection to the outside of the brain. A completely passive, wireless device that does not require on-board power for active transmission but that still facilitates remote detection could open the door for mass-scale direct recording of action potentials and transform the way we acquire brain signals. We present a nanofabricated coil that forms a neuroelectromagnetic junction, yielding a highly enhanced magnetic field transduction of electrophysiology. We show that this micrometer-scale device enables remote magnetic detection of neuronal fields from the center of the coil using room temperature superconducting quantum interference device (SQUID) microscopy. Further, time-locked stimulation in conjunction with magnetometry demonstrates thresholding behavior that affirms the viability of the technology for detection with no requirement for wires or on-board power. This strategy may permit unprecedented detection of electrophysiology using magnetoencephalography and magnetic resonance imaging.

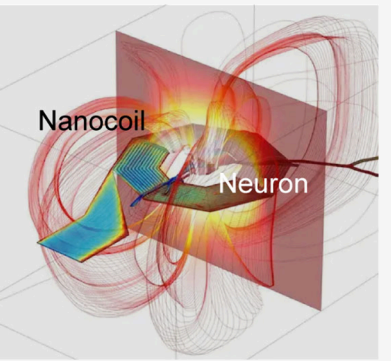


**KEYWORDS:** *Electrophysiology, Wireless, Nanocoils, SQUID, Magnetoencephalography, Magnetic Resonance Imaging*



Technologies for accessing the central nervous system are accelerating toward completely injectable probes that interact with noninvasive readout modalities for detection outside of the brain.[1−13] Neuronal currents are usually measured and amplified by invasive tethered devices.[14] Quantification of neuronal magnetic field perturbations resulting from these currents, for the purposes of detection by noninvasive modalities, has been explored both theoretically and experimentally.[15−18] Contemporary estimates place magnetic flux density near dendrites at 1 nT or lower, falling to zero very quickly within less than 1 $\mu$m from the plasma membrane.[15] These are considered too minute for detection based on spatiotemporal resolution, neuronal asynchrony, and theoretical sensitivity considerations.[19] Arrays of superconducting quantum interference devices (SQUIDs) and more recent optically pumped magnetometers are used for magnetoencephalography (MEG) to detect fields with a magnitude of 0.1 pT or higher ∼10 mm outside of the brain, but they require synchronous population activity from at least ten thousand cells in spatially constrained cortical columns tangentially aligned to the magnetic detectors.[18,20]

Developing cellular-scale elements that adhere to a small number of neurons and amplify neuronal magnetic fields in situ can present a way to overcome spatial and sensitivity limitations and empower functional magnetic resonance imaging (fMRI) and MEG to directly detect deep neuronal currents with precision. Here, we present a strategy whereby nanofabricated gold electromagnetic coils (nanocoils) can be tightly interfaced with excitable cells, resulting in a neuro-electromagnetic junction that enables magnetic detection of electrophysiological currents at submillisecond temporal resolution (Figure 1a,b).

We fabricated suitable devices using nanometer-scale electron beam lithography on top of silicon oxide on high resistivity silicon (>5000 Ω·cm) (Figure 1c). A 10-turn coil pattern with 100−200 nm conducting lines interspaced by 700−800 nm (Figure 1d, left and upper right panels) was patterned using direct write followed by deposition of Ti/Au (10/100 nm) for a coil turn aspect ratio of 1:1. The prototype has an estimated direct current (DC) inductance of 5.7−7.2 nH according to common models,[12,21] and a sheet resistance of 2.87 kΩ. For this study we used a large (width = 30 $\mu$m) exposed Ti/Au (10/300 nm) ground reference pad to face the extracellular electrolyte solution and protruding nanopillars at the neuronal interface pad to increase cell−device coupling[14,22] (Figure 1d, bottom right). This configuration is predicted to generate a relatively large differential potential (>5 mV) between the pads in response to an emulated neuronal action

**Received:** June 12, 2024
**Revised:** September 20, 2024
**Accepted:** September 20, 2024
**Published:** September 25, 2024

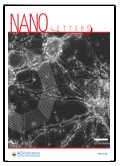





https://doi.org/10.1021/acs.nanolett.4c02784
*Nano Lett.* 2024, 24, 13147−13152

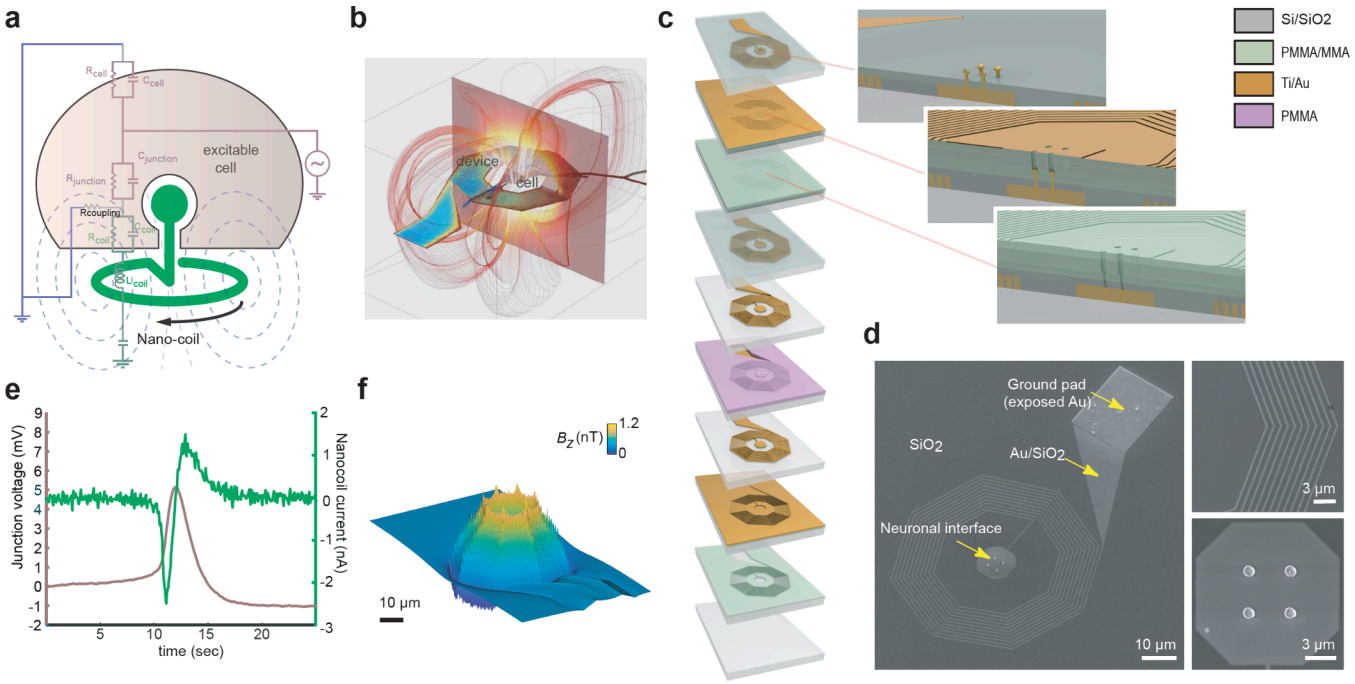


**Figure 1.** Nanocoil for magnetic sensing of neural electrical activity. (a) Equivalent circuit of the junction between nanocoil and excitable cell. (b) Neuroelectromagnetic junction. (c) Nanofabrication diagram. Left: fabrication process relies on direct e-beam write and Ti/Au deposition. Right: nanopillars on the interface pad for high coupling between cell and device. (d) Nanofabricated coil element consists of 10-turn coil structure electrically isolated from the electrolyte by silicon oxide, a neuronal interface pad with protruding exposed gold nanopillars, and a large gold reference pad facing the extracellular solution. Top right: coil structure with a turn conductor width of 100−200 nm. Bottom right: example of a neuronal interface pad with four protruding elements (width/height of ∼300 nm). (e) Circuit simulations indicate a junction potential of >5 mV, resulting in a nanocoil current of >4 nA (green trace) in response to input of emulated 80 mV intracellular action potential (brown trace). (f) Finite element analysis of the magnetic field distribution within the nanocoil during firing.

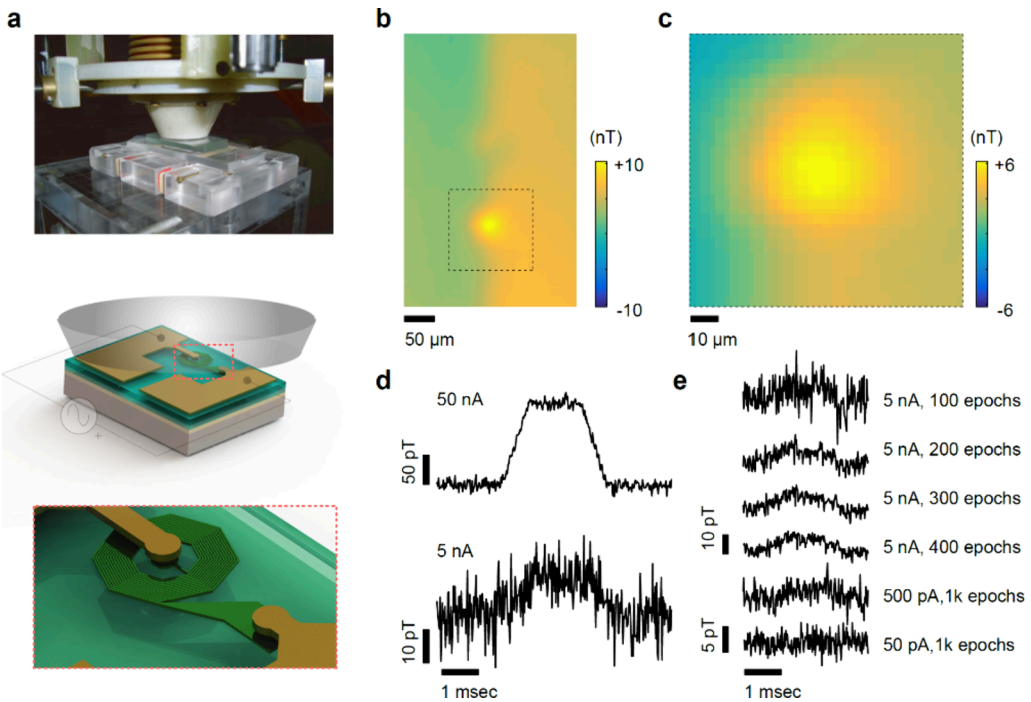


**Figure 2.** Magnetic field strength measurements of biologically relevant currents in a nanofabricated coil. (a) Experimental configuration of magnetic field detection using superconducting quantum interference device (SQUID) microscopy. (b) High-resolution magnetic field map in response to large direct current (1 $\mu$A). (c) Close-up view of dashed square in (b). (d) Measurements of magnetic fields in response to 0.5 kHz, 20% duty cycle current injection. Traces shown were averaged 50 times. (e) Magnetic field measurements of sub-nA currents, typical of neural activation. Device sensitivity of up to 500 pA yielding 5 pT fields has been observed. All measurements were performed in phosphate-buffered saline.



https://doi.org/10.1021/acs.nanolett.4c02784
Nano Lett. 2024, 24, 13147−13152

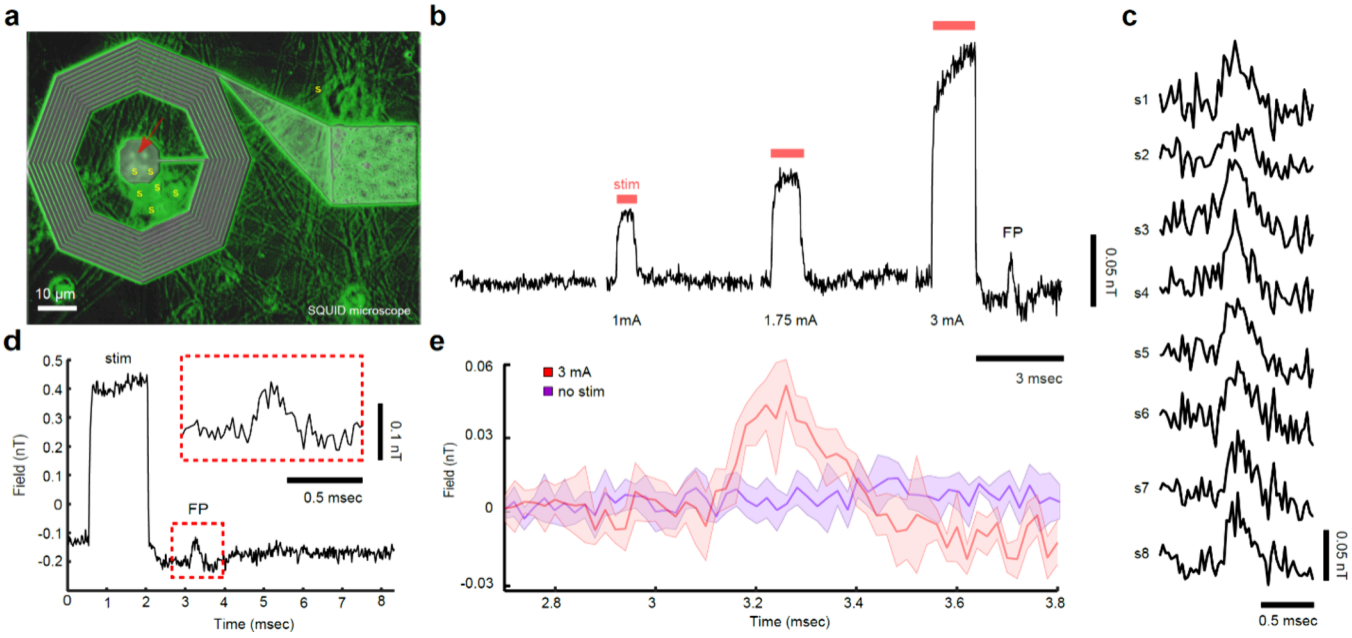


**Figure 3.** Magnetic field measurements of neural activity from several neurons cultured on a nanocoil. (a) Primary cortical neurons grown on nanocoil (s: somata aggregating at interface pad marked by red arrow). (b) Neurons were stimulated (red), resulting in field potential (FP) detected magnetically by SQUID microscopy at the center of the nanocoil. Shown are four epochs of increasing stimuli to a suprathreshold firing event (right-hand side, FP). (c) Measurements from 8 separate stimulation trials. (d) FP of amplitudes up to 0.1 nT were detected. (e) Average responses ($n$ = 8) to stimulation (3 mA, red) vs no stim (purple).

potential (~80 mV), resulting in a current amplitude of >4 nA (Figure 1e). This amounts to a maximum magnetic field strength of 1.2 nT in the middle of the coil (Figure 1f) and a very large spatial enhancement of the transduced magnetic field output within a typical volume (40 × 40 × 10 $\mu$m) of over 250 times higher than the intrinsic neuronal field strength (0.64 nT vs 2.5 pT, respectively) based on finite element analysis.[12]

We measured the strength of magnetic fields detected remotely (0.2 mm distance) arising from fields developing in the nanocoil during physiologically relevant current injections (Figure 2a) using superconducting quantum interference device (SQUID) microscopy at room temperature[23,24] with a spatial resolution of 5 $\mu$m and a magnetic field spectral power density of $S_B^{1/2} < 1.5$ pT/Hz$^{1/2}$ (Figure 2a, top). Application of a 1 $\mu$A (DC) current yielded remotely detected field strengths ranging between 5 and 10 nT from within the radius of the coil (Figure 2b,c). Alternating currents (0.5 kHz) at millisecond durations and at amplitudes ranging between 500 pA and 50 nA resulted in remotely detected magnetic field strength values ranging between 5 pT and 0.15 nT (Figure 2d,e). Application of currents of 50 pA or smaller yielded no measurable magnetic field averaged across 1000 epochs, suggesting this value to be the sensitivity limit of our system (Figure 2e, bottom).

To verify the presence of a neuron−nanocoil junction able to transduce neural activity into a detectable magnetic field, we stimulated primary cortical neurons cultured on the device and performed SQUID microscopy measurements of the resulting time-locked magnetic field in the center of the coil (Figure 3). Prior to cell culture, devices were chemically functionalized with polyethylenimine (PEI) to facilitate close adhesion to primary rat cortical neurons cultured on the device. The cells aggregated at protruding mushrooms of the interface pad (Figure 3a, arrow). We stimulated the neurons electrically by an Ag/AgCl electrode in the bath for 1−2 ms at 1−3 mA (Figure 3b, red: stim). Neuronal field potential response was detected magnetically ~1 ms following sufficient stimulation (Figure 3b, FP). No response was detected following subthreshold stimulation pulses (Figure 3b). The magnetic field amplitude recorded remotely was ~0.05 nT 150 $\mu$m above the coil (Figure 3b, rightmost trace) consistently between 8 individual stimulation sequences (Figure 3c).

Field potentials were detected magnetically with amplitudes of up to 0.1 nT, 0.2 mm above the sample (Figure 3d). Response to a 3 mA stimulation was in the form of spikes with an average maximum amplitude of 0.083 ± 0.013 nT, 1.31 ± 0.06 ms following stimulus, a rise time of 0.240 ± 0.100 ms, a decay time of 0.180 ± 0.060 ms, and undershoot lasting 0.440 ± 0.520 ms (Figure 3b−e, $n$ = 8). No spikes were recorded without stimulus, with a maximum recorded RMS amplitude of 0.038 ± 0.002 nT for each 0−10 ms epoch (Figure 3b, right), similar to the basal RMS noise level of 0.048 ± 0.017 nT without stimulation, showing no significant difference ($P$ = 0.178).

The approach presented here provides a means for transducing neuronal firing into fields that can be detected remotely by widely available magnetometry instrumentation. The junction between neurons and our nanocoils operates similarly to a neuron−electrode junction but leverages the coil geometry for greatly enhancing the magnetic field induced by neuronal ionic fluctuations with a 250-fold spatial enhancement compared with intrinsic neuronal fields. Neuronal excitation manifests as mobilization of ionic charge that induces capacitive effects at the Au Helmholtz double layer, followed by mobilization of electrons in the electrode substrate.[14] Intrinsically minute and spatially constrained magnetic fields produced by the resulting current flow are summed cumulatively by the nanocoil design in proportion to its turn density. This prototype can be further optimized by maximizing turn density while maintaining minimal parasitic


https://doi.org/10.1021/acs.nanolett.4c02784
Nano Lett. 2024, 24, 13147−13152

capacitance, an effort that would be limited only by the spatial resolution of current nanoscale lithography techniques relative to the microscale diameter of living cells. This could potentially allow for measurements from single neurons. Another important consequence of the nanocoil approach is the ability to redirect magnetic flux lines and enable measurements from regions that are not tangentially aligned with magnetic detectors. MEG is primarily sensitive to activity originating in cortical sulci rather than gyri, precluding comprehensive readouts.[20] Implanting dense nanocoil arrays in diverse regions and conformations can circumvent limitations inherent to MEG sensors and orientation dependency on $B_1$ fields common to MRI RF receive coils. With a ∼250-fold spatial enhancement per device and assuming moderately aligned multiple implanted sensor arrays at a density of one device per 0.01−0.02 $m^3$, we expect cumulative fields of 1−10 pT at distances of 20 mm using SQUID-based MEG recordings, surpassing the detection of naturally occurring magnetic fields by more than an order of magnitude. Nonetheless, orientation-specific implantation deep in the brain is nontrivial and might require advanced microsurgical injection or magnetic field-based localization techniques.[13,25] Further, fabrication on flexible substrates[26] can provide anatomical conformity with brain structure and amplify signals that were thus far undetected. In comparison with current state-of-the-art recording technologies such as high density wired neuropixel devices[27,28] or emerging wireless electromagnetic, acoustic, and optical probes,[13,29,30] the nanocoil approach is expected to eliminate power transmission requirements altogether and greatly reduce adverse tissue effects. Future optimizations, however, will be required to enable addressability for comparable high density recording abilities and fully recruit the technology for neuroscience and neural engineering applications such as direct biofeedback-based neurotherapeutics and a minimally invasive brain machine interface.

## EXPERIMENTAL METHODS

**Equivalent Circuit Model.** The neuron−device interface was modeled as an equivalent circuit in PSpice (Cadence Design Systems, Inc., San Jose, California, USA). The resistance and capacitance of the cell were initialized to 100 MΩ and 10 nF, respectively. Similarly, junction resistance and capacitance were 10 MΩ and 0.1 pF, respectively. Leak resistance at the coupling between the junction and coil was set to 1 GΩ. Coil resistance, capacitance, and inductance were configured as 2.78 kΩ, 0 F, and 0.1 nH, respectively. $R$ and $C$ were also defined for the junctional (1 TΩ, 5 pF) and nonjunctional (1 TΩ, 50 pF) solution milleu. The time-dependent voltage of the cell was derived from patch clamp recordings and fed into the neuron model.

**Nanofabrication.** Devices were nanofabricated using electron beam lithography patterning followed by liftoff, similar to previous work.[12,31] Briefly, a $Si/SiO_2$ substrate was spin-coated at 3000 rpm for 30 s with a PMMA/MMA bilayer (catalog no. M310011-0500L1GL, Kayaku) and baked at 180 °C for 2 min to yield a typical resist thickness of 400 nm. Direct write of inductor patterns was then performed by electron beam lithography (Elionix, Tokyo, Japan), followed by the development of the resist using methyl isobutyl ketone/isopropyl alcohol (MIBK/IPA) (1:2). Ti/Au (1:10) was deposited by electron beam deposition followed by PMMA/MMA liftoff in ultrasonicated acetone (5 min) at room temperature. A silicon oxide insulating layer was deposited by plasma-enhanced chemical vapor deposition. An additional nanolithography step was performed using spin-coated PMMA as a barrier layer to define the ground pad and protruding pillars at the interface pad, followed by buffered oxide etching through the silicon oxide layer. Au protrusions were grown by electron beam deposition before a second layer of PMMA/MMA was lifted off.

**Cell Culture and Electrical Stimulation.** For cell culture, recording, and stimulation, we used methods described previously.[32,33] First, to hydrophilize the device, a small 50 μL droplet of phosphate-buffered saline (PBS) was placed over the device region. The nanocoils were incubated overnight at 37 °C and 5% $CO_2$. The PBS was then aspirated, and 50 μL droplets of either polyethylenimine (PEI) or poly-D-lysine with 4 μg/mL laminin were placed on the devices, which were again incubated for 60 min at 37 °C. The devices were washed three times with PBS. Primary neurons were retrieved from live dissection at a concentration of 10 million cells/mL. The cells were diluted to 4 million cells/mL using unwarmed plating medium and plated onto devices that were incubated for 4 h. The plating medium was removed, and medium changes were performed 2−3 times per week thereafter until experiments were performed on DIV 13. Neurons were stimulated electrically by a bipolar Ag/AgCl electrode fabricated with two Teflon-coated wires (178 μm coated, 127 μm uncoated) and a ground wire placed inside the cell solution bath. Stimulation was performed at 10 Hz for 1−2 ms at 1−3 mA using a high current stimulus isolator (World Precision Instruments, Sarasota, Florida, USA).

**Finite Element Modeling.** Simulations of the device magnetic response were performed in a COMSOL Multiphysics simulation environment (COMSOL Inc., Stockholm, Sweden). An optimized coil pattern described previously[12] and used here for nanofabrication was imported to COMSOL and extruded 500 nm along the $z$-axis. The dielectric layer was 900 nm thick above the substrate, providing 400 nm of separation between the device and the electrode contacts. Cylinders with a diameter of 8 μm were extruded through the dielectric over the interface pad and ground pad, and microfabricated electrode contacts were patterned above the dielectric and extruded to a thickness of 400 nm. The device had 14 turns, resulting in an open core percentage of 46.2%. The electrical properties of the device and microfabricated electrode contacts were set to those of gold, $\varepsilon = 1$, $\mu = 1$, and $\sigma = 45.6 \times 10^6$ S/m. The electrical properties of the substrate and dielectric layer in the model were set to those of silicon dioxide ($SiO_2$), $\varepsilon = 4.2$, $\mu = 1$, $\sigma = 1 \times 10^{-15}$ S/m. The electrical properties of the space above the device were set to those of air, $\varepsilon = 1$, $\mu = 1$, $\sigma = 0.7$ S/m. All device geometries were tested using an input current of 3 mA. The current was input through the outside face of the microfabricated electrode contact, connecting to the interface pad at the center of the inductor. The outside face of the electrode contact above the ground pad was used as the ground port.

## AUTHOR INFORMATION

### Corresponding Authors

**Alan Jasanoff** − *Department of Biological Engineering, Massachusetts Institute of Technology, Cambridge, Massachusetts 02108, United States; Department of Brain & Cognitive Sciences and Department of Nuclear Science & Engineering, Massachusetts Institute of Technology, Cambridge, Massachusetts 02139, United States;*



https://doi.org/10.1021/acs.nanolett.4c02784
*Nano Lett.* 2024, 24, 13147−13152

orcid.org/0000-0002-2834-6359; Email: jasanoff@mit.edu

**Aviad Hai** − *Department of Biomedical Engineering and Department of Electrical and Computer Engineering, University of Wisconsin-Madison, Madison, Wisconsin 53706, United States; Department of Biological Engineering, Massachusetts Institute of Technology, Cambridge, Massachusetts 02108, United States;* orcid.org/0000-0002-4556-3048; Email: ahai@wisc.edu

### Authors

**Ilhan Bok** − *Department of Biomedical Engineering and Department of Electrical and Computer Engineering, University of Wisconsin-Madison, Madison, Wisconsin 53706, United States;* orcid.org/0000-0002-4481-7843

**Jack Phillips** − *Department of Biomedical Engineering, University of Wisconsin-Madison, Madison, Wisconsin 53706, United States*

**Tianxiang Zhu** − *Department of Electrical and Computer Engineering, University of Wisconsin-Madison, Madison, Wisconsin 53706, United States*

**Jennifer Lu** − *Department of Biological Engineering, Massachusetts Institute of Technology, Cambridge, Massachusetts 02108, United States*

**Elizabeth Detienne** − *Department of Biological Engineering, Massachusetts Institute of Technology, Cambridge, Massachusetts 02108, United States*

**Eduardo Andrade Lima** − *Department of Earth and Planetary Science, Massachusetts Institute of Technology, Cambridge, Massachusetts 02139, United States*

**Benjamin P. Weiss** − *Department of Earth and Planetary Science, Massachusetts Institute of Technology, Cambridge, Massachusetts 02139, United States*

Complete contact information is available at: https://pubs.acs.org/10.1021/acs.nanolett.4c02784

### Author Contributions

A.H., A.J., E.A.L., and B.P.W. designed the research. A.H. and J.L. performed device fabrication. A.H. and E.D. performed cortical cell cultures. A.H. and E.A.L. performed magnetic measurements. A.H. and I.B. analyzed the data. J.P. performed computational modeling. A.H., I.B., J.P., T.Z., and A.J. wrote the manuscript.

### Notes

The authors declare no competing financial interest.

## ■ ACKNOWLEDGMENTS

This research was funded by NIH Grants K01 EB027184 and DP2 NS122605 to A.H. and Grants R01 NS76462, R01 DA038642, and U01 NS904051 to A.J. We thank Dr. Yingxi Lin for providing resources and cortical cells.

## ■ ABBREVIATIONS

MEG, magnetoencephalography; MRI, magnetic resonance imaging; SQUID, superconducting quantum interference device

## ■ REFERENCES

(1) Gutruf, P.; et al. Fully implantable optoelectronic systems for battery-free, multimodal operation in neuroscience research. *Nature Electronics* **2018**, *1*, 652−660.

(2) Trevathan, J. K.; Baumgart, I. W.; Nicolai, E. N.; Gosink, B. A.; Asp, A. J.; Settell, M. L.; Polaconda, S. R.; Malerick, K. D.; Brodnick, S. K.; Zeng, W.; Knudsen, B. E.; McConico, A. L.; Sanger, Z.; Lee, J. H.; Aho, J. M.; Suminski, A. J.; Ross, E. K.; Lujan, J. L.; Weber, D. J.; Williams, J. C.; Franke, M.; Ludwig, K. A.; Shoffstall, A. J. An Injectable Neural Stimulation Electrode Made from an In-Body Curing Polymer/Metal Composite. *Adv. Healthcare Mater.* **2019**, *8*, No. 1900892.

(3) Lee, T.; Cai, L. X.; Lelyveld, V. S.; Hai, A.; Jasanoff, A. Molecular-Level Functional Magnetic Resonance Imaging of Dopaminergic Signaling. *Science* **2014**, *344*, 533−535.

(4) Hai, A.; Jasanoff, A. Molecular fMRI. In *Brain Mapping: An Encyclopedic Reference*; Toga, A. W., Ed.; Academic Press, Waltham, Massachusetts USA, 2015; p 123−129. DOI: 10.1016/B978-0-12-397025-1.00013-0.

(5) Hai, A.; Cai, L. X.; Lee, T.; Lelyveld, V. S.; Jasanoff, A. Molecular fMRI of Serotonin Transport. *Neuron* **2016**, *92*, 754−765.

(6) Hai, A.; Spanoudaki, V. C.; Bartelle, B. B.; Jasanoff, A. Wireless resonant circuits for the minimally invasive sensing of biophysical processes in magnetic resonance imaging. *Nat. Biomed Eng.* **2019**, *3*, 69−78.

(7) Bricault, S.; Barandov, A.; Harvey, P.; DeTienne, E.; Hai, A.; Jasanoff, A. Image-guided neural activity manipulation with a paramagnetic drug. *Nat. Commun.* **2020**, *11*, 136.

(8) Seo, D.; et al. Wireless Recording in the Peripheral Nervous System with Ultrasonic Neural Dust. *Neuron* **2016**, *91*, 529−539.

(9) Piech, D. K.; et al. A wireless millimetre-scale implantable neural stimulator with ultrasonically powered bidirectional communication. *Nature Biomedical Engineering* **2020**, *4*, 207−222.

(10) Szablowski, J. O.; Lee-Gosselin, A.; Lue, B.; Malounda, D.; Shapiro, M. G. Acoustically targeted chemogenetics for the non-invasive control of neural circuits. *Nature Biomedical Engineering* **2018**, *2*, 475−484.

(11) Bok, I.; Haber, I.; Qu, X.; Hai, A. In silico assessment of electrophysiological neuronal recordings mediated by magnetoelectric nanoparticles. *Sci. Rep* **2022**, *12*, 8386.

(12) Phillips, J.; Glodowski, M.; Gokhale, Y.; Dwyer, M.; Ashtiani, A.; Hai, A. Enhanced magnetic transduction of neuronal activity by nanofabricated inductors quantified via finite element analysis. *J. Neural Eng.* **2022**, *19*, 046003.

(13) Bok, I.; Vareberg, A.; Gokhale, Y.; Bhatt, S.; Masterson, E.; Phillips, J.; Zhu, T.; Ren, X.; Hai, A. Wireless agents for brain recording and stimulation modalities. *Bioelectronic Medicine* **2023**, *9*, 20.

(14) Spira, M. E.; Hai, A. Multi-electrode array technologies for neuroscience and cardiology. *Nat. Nanotechnol.* **2013**, *8*, 83−94.

(15) Xue, Y.; Gao, J.-H.; Xiong, J. Direct MRI detection of neuronal magnetic fields in the brain: Theoretical modeling. *NeuroImage* **2006**, *31*, 550−559.

(16) Caruso, L.; Wunderle, T.; Lewis, C. M.; Valadeiro, J.; Trauchessec, V.; Trejo Rosillo, J.; Amaral, J. P.; Ni, J.; Jendritza, P.; Fermon, C.; Cardoso, S.; Freitas, P. P.; Fries, P.; Pannetier-Lecoeur, M. In Vivo Magnetic Recording of Neuronal Activity. *Neuron* **2017**, *95*, 1283.

(17) Sadleir, R. J.; et al. Direct detection of neural activity in vitro using magnetic resonance electrical impedance tomography (MREIT). *Neuroimage* **2017**, *161*, 104−119.

(18) Boto, E.; et al. Moving magnetoencephalography towards real-world applications with a wearable system. *Nature* **2018**, *555*, 657−661.

(19) Bandettini, P. A.; Petridou, N.; Bodurka, J. Direct detection of neuronal activity with MRI: Fantasy, possibility, or reality? *Appl. Magn. Reson.* **2005**, *29*, 65−88.

(20) Baillet, S. Magnetoencephalography for brain electrophysiology and imaging. *Nat. Neurosci* **2017**, *20*, 327−339.

(21) Mohan, S. S.; del Mar Hershenson, M.; Boyd, S. P.; Lee, T. H. Simple accurate expressions for planar spiral inductances. *IEEE Journal of Solid-State Circuits* **1999**, *34*, 1419−1424.

(22) Hai, A. In-Cell Recording and Stimulation by Engulfment Mechanisms. In *Nanotechnology and Neuroscience: Nano-electronic, Photonic and Mechanical Neuronal Interfacing*; De Vittorio, M.,

Martiradonna, L., Assad, J., Eds.; Springer, New York, New York, USA, 2014; p 45−70. DOI: 10.1007/978-1-4899-8038-0_3.
(23) Fong, L. E.; et al. High-resolution imaging of cardiac biomagnetic fields using a low-transition-temperature superconducting quantum interference device microscope. *Appl. Phys. Lett.* **2004**, *84*, 3190−3192.
(24) Weiss, B. P.; Lima, E. A.; Fong, L. E.; Baudenbacher, F. J. Paleomagnetic analysis using SQUID microscopy. *Journal of Geophysical Research: Solid Earth* **2007**, *112*, 1.
(25) Khalifa, A.; Lee, S.; Molnar, A. C.; Cash, S. Injectable wireless microdevices: challenges and opportunities. *Bioelectronic Medicine* **2021**, *7*, 19.
(26) Viventi, J.; et al. Flexible, foldable, actively multiplexed, high-density electrode array for mapping brain activity in vivo. *Nat. Neurosci* **2011**, *14*, 1599−1605.
(27) Paulk, A. C.; et al. Large-scale neural recordings with single neuron resolution using Neuropixels probes in human cortex. *Nat. Neurosci* **2022**, *25*, 252−263.
(28) Topalovic, U.; et al. A wearable platform for closed-loop stimulation and recording of single-neuron and local field potential activity in freely moving humans. *Nat. Neurosci* **2023**, *26*, 517−527.
(29) Lee, J.; et al. Neural recording and stimulation using wireless networks of microimplants. *Nat. Electron* **2021**, *4*, 604−614.
(30) Bhatt, S.; et al. Wireless in vivo recording of cortical activity by an ion-sensitive field effect transistor. *Sens. Actuators, B* **2023**, *382*, No. 133549.
(31) Bok, I.; Ashtiani, A.; Gokhale, Y.; Phillips, J.; Zhu, T.; Hai, A. Nanofabricated high turn-density spiral coils for on-chip electro-magneto-optical conversion. *Microsyst Nanoeng* **2024**, *10*, 44.
(32) Ren, X.; Bok, I.; Vareberg, A.; Hai, A. Stimulation-mediated reverse engineering of silent neural networks. *J. Neurophysiol* **2023**, *129*, 1505−1514.
(33) Vareberg, A. D.; Bok, I.; Eizadi, J.; Ren, X.; Hai, A. Inference of network connectivity from temporally binned spike trains. *Journal of Neuroscience Methods* **2024**, *404*, No. 110073.



https://doi.org/10.1021/acs.nanolett.4c02784
*Nano Lett.* 2024, 24, 13147−13152